Available online at www.sciencedirect.com
ScienceDirect
Diamond & Related Materials 16 (2007) 6–11
DIAMOND AND RELATED MATERIALS
www.elsevier.com/locate/diamond

Characterization of energy levels related to impurities in epitaxial 4H-SiC ion implanted p^+n junctions

David Menichelli [a,b], Monica Scaringella [a,b], Francesco Moscatelli [c,d], Mara Bruzzi [a,b,*], Roberta Nipoti [c]

[a] *Dipartimento di Energetica, Via S. Marta 3, 50139 Florence, Italy*
[b] *INFN Firenze, via G. Sansone 1, 50518, Sesto Fiorentino (FI), Italy*
[c] *CNR-IMM Sezione di Bologna, via Gobetti 101, 40129 Bologna, Italy*
[d] *DIEI and INFN, Università di Perugia, via G. Duranti 93, 06125 Perugia, Italy*

Received 6 April 2005; received in revised form 14 March 2006; accepted 17 March 2006
Available online 16 May 2006

Abstract

The distribution of energy levels within the bandgap of epitaxial 4H-SiC p^+/n junctions was studied. The junction was obtained by Al ion implantation on a nitrogen doped n-type epitaxial substrate. Thermally stimulated currents/capacitance (TSC/TSCAP) as well as current/capacitance deep level transient spectroscopy (I- and C-DLTS) were carried out over a wide temperature range (20–400 K). The two TSC/DLTS peaks associated with N-doping were detected for the first time and their trap signatures determined. Two hole traps relating to deep and shallow boron confirm that a boron contamination occurred during crystal growth. A negligible concentration of the $Z_{1/2}$ level, which is usually the dominant level produced by irradiation of ion implant, was measured. The concentrations of all observed traps were significantly lower than nitrogen one, which determines the doping. This evidence supports the high quality of the processed junctions, making these devices particularly attractive for future use in particle detection as well as in optoelectronic applications.

PACS: 29.40.Wk Solid-state detectors; 71.55.Ht Other nonmetals (impurity and defect levels); 81.05.Hd Material science: other semiconductors; 61.72.Ji Point defects: vacancies, interstitials, color centers, etc. and defect clusters
Keywords: Silicon carbide (SiC); Implantation; Defect characterization; Detectors

1. Introduction

Single crystal silicon carbide (SiC) recently generated great interest because of its optical and electrical transport properties, in particular for high power [1], high temperature [2], high frequency applications [3] and radiation detection [4]. Schottky diodes fabricated on high quality epitaxial SiC substrates show promising performance [2,5]; however, a technological process based on Schottky barriers is unsuitable for the production of complex radiation detectors featuring an on-board integrated electronics circuit. In the latter case, p/n junctions are needed together with MOSFET devices. Many research groups have analyzed ion implanted p^+/n junctions [6–9] with low reverse leakage current and high breakdown voltages. To assess the production of junction-based SiC detectors, a detailed study on the crystalline quality of the epilayer and of the defect distribution in the device bulk is nevertheless mandatory. Traps and generation-recombination centers dominate the leakage current, effective doping concentration and charge collection properties of SiC diodes. Such defects, which are not yet unequivocably identified in spite of many studies dedicated to this investigation may be native or induced by processes used in making the device. This paper aims to give a contribution to this field.

The characterization of ion implanted p^+/n junctions has been carried out by capacitance [10] and current [11,12] deep level transient spectroscopy (C-DLTS and I-DLTS), thermally stimulated current (TSC) and thermally stimulated capacitance (TSCAP) [13,14]. The comparison to data in literature, when

* Corresponding author. Dipartimento di Energetica, Via S. Marta 3, 50139 Florence, Italy. Tel.: +39 055 4796350; fax: +39 055 4796342.
E-mail address: mara.bruzzi@cern.ch (M. Bruzzi).

0925-9635/$ - see front matter © 2006 Published by Elsevier B.V.
doi:10.1016/j.diamond.2006.03.008

available, allowed us to hypothesize which defects were due to the technological steps applied for the bipolar diode construction.

2. Experimental procedures

2.1. Samples

The samples studied in this work were ion implanted p^+/n 4H-SiC diodes, produced in the frame of the collaboration between INSA-Cegely (Lyon, France) and CNR-IMM (Bologna, Italy). A ⟨0001⟩ 8° miss-cut oriented 4H-SiC *n-type* epitaxial wafer was used for this study. The p^+ anodes were obtained by aluminum ion (Al^+) implantation in the epilayer 40 μm thick, n^- (nitrogen N) doped with density $N_D=1.1\times10^{15}$ cm^{-3}, as measured by *C–V* profiles. Al^+ multiple energy implantation process with energies in the range 25–300 keV and fluence of $0.9–8\times10^{14}$ cm^{-2} was used to produce an almost box shaped Al 4×10^{19} cm^{-3} doping profile 0.45 μm thick. The implantation temperature was 300 °C. The implanted wafer was annealed in an inductively heated J.I.P.ELEC™ furnace at 1650 °C for 30 min in high purity Ar gas at a partial pressure just above the atmospheric pressure. Al/Ti and Ni alloyed ohmic contacts were made on the p^+ anode and the n^+ base ($\sim10^{18}$ cm^{-3}), respectively. The contact alloying process was done at 1000 °C for 2 min in vacuum [15]. Diodes of different areas were made. Circular diodes with 1mm diameter were used for the spectroscopy measurements presented in this paper. Two diodes with identical *I–V* curves were connected in parallel to increase the active area and, in turn, improve the signal to noise ratio during measurements. The reverse characteristics of each diode features a leakage current equal to $\sim10^{-12}$ A at 100 V and a breakdown voltage equal to 1.3 kV in air and 4–4.8 kV in Galden or SF6 [16].

2.2. Experimental setup

In C-DLTS measurements, capacitance transients were converted into voltage by a SULA Tech. Deep Level Spectrometer, with 1 MHz test signal frequency and 50 mV amplitude. Then a digital oscilloscope (Tektronix TDS520D) performed the acquisition of the transients at selected sampling times. In I-DLTS experiments, the spectrometer is replaced by a pulse generator (Systron Donner 110D) providing reverse bias and pulsed injection, and by a custom readout circuit [17]. In TSCAP measurements, capacitance is measured directly by the SULA spectrometer. An HP4284A LCR meter measures the *C*(*V*) characteristics at room temperature. Thermally stimulated currents (TSC) experiments were carried out using an apparatus similar to the C-DLTS one, where the spectrometer is replaced by the Keithley 6517A electrometer, providing sample bias, low temperature forward injection and current reading.

Two possible schemes for sample cooling were used in our measurements. In the first, the sample sits inside a vacuum chamber where a pressure below 10^{-3} mbar is maintained. The cryogenerator (Officine Galileo K1) cools the sample-holder, while a resistor wound around it heats the sample. This cooling system allows one to reach the minimum temperature of 20 K. A constant heating rate β–slow enough not to affect the shape of the spectrum ($\beta\leq0.07$ K/s)–was always adopted in current and capacitance DLTS experiments. A second cooling was used to achieve lower temperatures. It also ensures a better thermal coupling between sample and temperature sensor. The sample holder, mounted on a long steel hollow tube placed inside a liquid He dewar at different heights above the liquid surface, achieves temperatures between 4.2 K and room temperature.

All the measurements were carried out at 10 V reverse bias and priming was performed using a forward bias limited to a 3 mA forward current. Taking into account of the depletion layer thickness in the p^+n junction (the built-in potential is 2.7 V), the doping density of the epilayer, the 4H-SiC relative dielectric constant ($\varepsilon_r=9.7$) and the specimen polarization during the measurements, the traps responsible of the spectra presented in this paper stayed in a 4H-SiC 4-μm-thick layer.

3. Experimental results and discussion

The capacitance DLTS spectrum measured in the range 30–220 K is shown in Fig. 1. Sampling times and duration of injection pulse were $t_1=5$ ms, $t_2=45$ ms and $t_p=10$ ms, respectively. Several peaks were observed in the experimental C-DLTS spectrum: two negative peaks caused by electron traps labeled E_2 and E_3 and two positive peaks corresponding to hole traps labeled H_1 and H_2. The bottom of Fig. 1 shows the junction capacitance versus temperature *C*(*T*) measured without carrier injection. The corresponding vertical scale is plotted on the right axis. When decreasing *T* below 60 K, the junction capacitance sharply decreases and then reaches a plateau value corresponding to the geometric capacitance $C_g\cong8$ pF. From *C*(*T*) measurements, we infer that the ionization of nitrogen occurs in the range 30–60 K, where the junction is formed. The E_2 peak

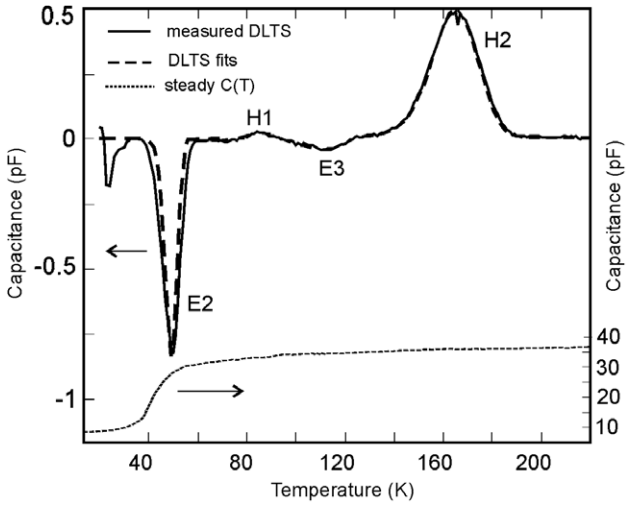

Fig. 1. DLTS capacitance spectrum measured in the range 20–220 K (solid line). The trap signature fit (dashed lines) is superimposed to the measured values (solid line). Sampling times and duration of pulse injection are $t_1=5$ ms, $t_2=45$ ms and $t_p=10$ ms, respectively. The steady state capacitance *C*(*T*) is shown in the bottom of the figure (dotted line). The vertical scale corresponding to the latter curve is shown on the right axis. All the measurements were made with $V_{rev}=10$ V.

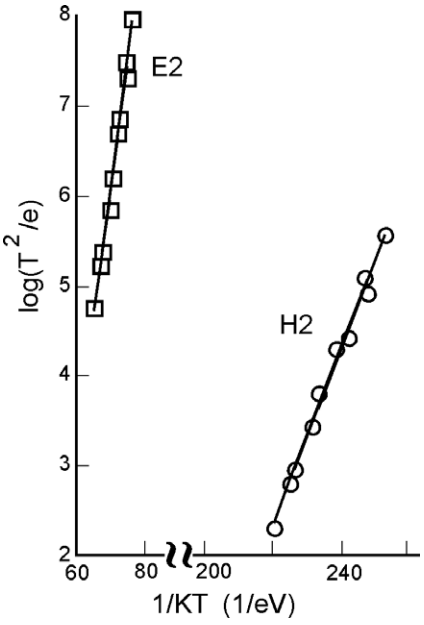

Fig. 2. Arrhenius plots obtained from C-DLTS spectra measured with different sampling times. The squared markers refer to the E_2 peak and the circles to the H_2 peak.

falls in this range too, which suggests a relationship of the E_2 peak with nitrogen. It is known that nitrogen produces two energy levels close to 50 meV and 100 meV. These levels were inferred in past by different experimental evidences, as capacitance– and current–voltage measurements as a function of the temperature in the range 100–200 K [18], photoluminescence [19] and Hall effect measurements [20–22]. The two nitrogen levels correspond to the substitutional hexagonal and cubic sites in the lattice, respectively.

A variety of C-DLTS measurements were carried out using different sampling times: resulting Arrhenius plots of the peaks E_2 and H_2 are shown in Fig. 2. Here $\ln(T_p^2/e)$ is plotted versus $1/K_B T_p$, where T_p is the peak temperature of the C-DLTS signal, K_B is the Boltzmann constant and e the emission coefficient of the trap at the temperature T_p. The resulting trap parameters of E_2 are $E \cong 0.10$ eV and $\sigma \sim 10–200 \cdot 10^{-15}$ cm^2 . Even if these values are considered a first approximation (because the modification of junction capacitance during charge emission from traps is not negligible), they confirm that E_2 corresponds to the nitrogen level close to 100 meV. This energy level can produce a significant C-DLTS signal because the junction is already formed during the ionization of the shallower nitrogen level, which occurs at lower temperatures. On the contrary, the shallower nitrogen level cannot be observed because the junction forms after its ionization starts to occur.

From the Arrhenius plot, the signature of the H_2 peak was found to be: $E = 0.28 \pm 0.01$ eV, $\sigma \sim 0.2–1 \cdot 10^{-15}$ cm^2. This emission is associated with shallow boron. Many studies targeted boron because this impurity may be a p-type dopant for SiC [23–25]. Boron occupies both the silicon and the carbon sites with a preference for the Si site for samples grown with a low Si/C ratio [25,26]. This produces a deep acceptor center at E_V+ 0.55 eV and a shallow level at E_V+(0.26–0.30) eV. The deep

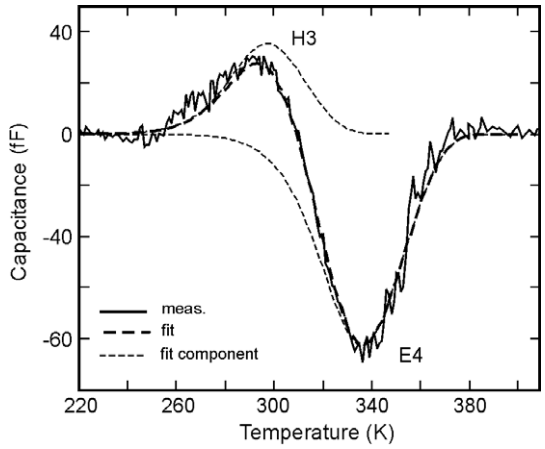

Fig. 3. DLTS capacitance spectrum measured around room temperature (solid line) using $t_1 = 1$ ms, $t_2 = 9$ ms, $V_{rev} = 10$ V and $t_p = 10$ ms. The two components H_3 and E_4 (thin dashed lines) accounts for the spectrum. The sum of these components is plotted with a smooth and thick dashed line.

boron peak usually appears at a temperature slightly lower than the $Z_{1/2}$ peak. Boron at a silicon site is usually associated with a shallow acceptor while boron at a carbon site is associated with a deep acceptor. Thus, H_2 may be related to shallow boron, which could have contaminated the sample during growth and processing. This relationship is reinforced by the observation of the deep boron peak described below. Note, however, that the cross section value measured by us is smaller than the value reported in [23] as calculated from minority carriers transient spectroscopy (MCTS) technique ($\sigma = 2 \cdot 10^{-14}–3 \cdot 10^{-13}$ cm^{-2}). Such a large σ value is not consistent with our measurements. Fig. 1 (dashed lines) shows the fit corresponding to the E_2 and H_2 trap parameters superimposed on the measured spectrum.

Two minor components in the C-DLTS spectra are observed close to room temperature. The spectrum measured in the range

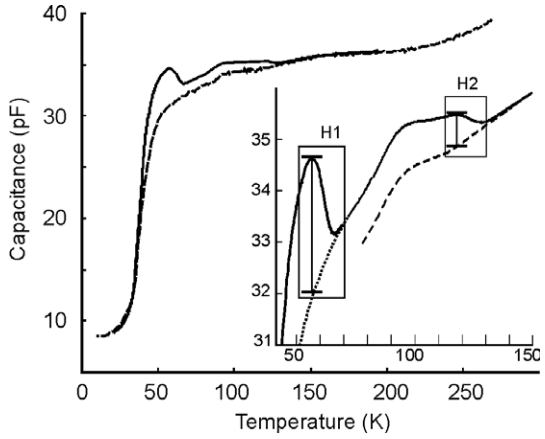

Fig. 4. A TSCAP spectrum (solid line) is compared to the $C(T)$ profile measured without performing any injection (dashed line). An enlargement of the region between 50 K and 150 K is shown in the inset. The emissions from two hole traps H_1 and H_2 are highlighted. An additional trace (dotted line) shows the measurement obtained by stopping the spectrum measurement at 70 K, cooling again and performing a new measurement without injection ($V_{rev} = 10$ V, $\beta = 0.15$ K/s). Injection: 1 min of forward bias ($i = 10$ mA). Vertical bars indicate the amplitude of capacitance transition ($C_f - C_i$) due to each trap.

220–400 K is shown in Fig. 3. The spectral feature observed in this temperature range is composed of a hole emission, labeled H_3, and an electron emission, E_4. We did not attempt to draw the Arrhenius plots of levels E_3 and H_1, or H_3 and E_4 because their signals are extremely weak and a reliable analysis based on Arrhenius plots cannot be carried out. We obtained a rough estimate of the E_3 signature by fitting the position and the linewidth of the C-DLTS peak. The result is: $E=0.15\pm0.1$ eV, $\sigma\sim10^{-17}$ cm^2. We will discuss H_1 later in conjunction with additional measurements. H_3 and E_4 were identified by comparing the fits produced by the signatures reported in literature. E_4 was fitted using the signature of the $Z_{1/2}$ center. The $Z_{1/2}$ DLTS peak near 300 K is often reported to be the dominant feature of SiC after ion implantation [27] or irradiation with different particles, such as electron and protons [28–30]. The corresponding deep level signature was $E=0.63$–0.67 eV, $\sigma=3$–$20\cdot10^{-15}$ cm^2. The measured concentration of $Z_{1/2}$ is usually in the range 10^{14}–10^{15} cm^{-3} depending on irradiation and annealing procedure. The $Z_{1/2}$ center is sometimes observed in non-irradiated epilayers [23,31]. It was suggested to be the superposition of the two-electron emission processes ($Z_1^{-/+}$and $Z_2^{-/+}$) from a negative-U system [32,33]. Although the study of the $Z_{1/2}$ center in 4H–SiC was reported quite extensively [34], the exact microscopic structure of this defect is still unknown. The current consensus is that the $Z_{1/2}$ center is related to a vacancy-type defect. H_3 relation to deep boron confirms that a boron contamination occurred during processing. In our samples, the concentrations of H_3 and E_3 were of the order of 10^{12} cm^{-3}.

Further information, complementary to those obtained from C-DLTS, was gained from TSCAP spectra shown in the main plot of Fig. 4 (solid line). The spectrum is compared to the capacitance profile $C(T)$ measured without any low temperature carrier injection. Below 20 K, $C(T)$ is fixed to the geometrical value. In the range 20–50 K, the nitrogen freeze out occurs, the junction settles and the capacitance reaches a value close to 30 pF. Above 50 K, the $C(T)$ characteristic exhibits a slow monotonic increase not related to charge emission from defect levels. The TSCAP spectrum, measured with low temperature carriers injection matches $C(T)$ above 150 K. On the contrary, at lower temperatures these two signals exhibit some differences, which are related to the discharge of traps H_1, H_2 and E_3. The monotonic growth of $C(T)$ is superimposed on the discharge of E_3, which produces an increase in capacitance as well. For this reason, the contribution of E_3 to the TSCAP spectrum is not evident. On the contrary, the hole emissions due to H_1 and H_2 produce a sharp decrease in capacitance that is easily recognized in Fig. 4. The transition due to H_1 is visible at 65 K. H_2 is related to the capacitance decrease above 100 K seen where the curve measured after carriers injection matches the background capacitance, because its position agrees with the signature obtained from DLTS. In the inset, the temperature range 50–150 K is enlarged and the capacitance transitions due to H_1 and H_2 discharge are indicated. An additional curve (dotted line) corresponding to a fractional annealing stage is shown in this plot. The measurement was obtained by stopping the spectrum measurement at 70 K, cooling down again and repeating a new

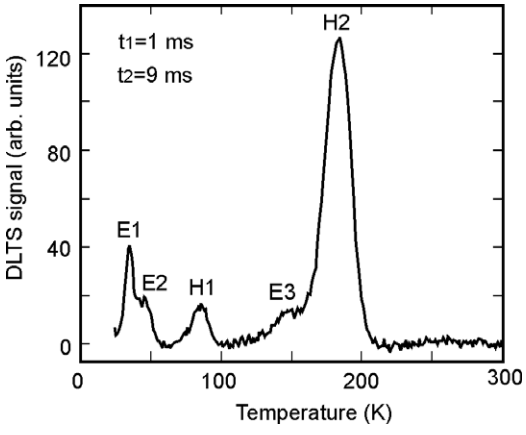

Fig. 5. I-DLTS spectrum measured in the range 20–300 K using the sampling times $t_1=1$ ms and $t_2=9$ ms ($V_{rev}=10$ V, $t_p=10$ ms).

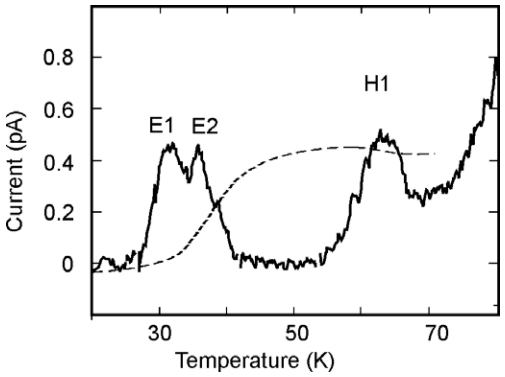

Fig. 6. TSC spectrum measured in the range 20–80 K with $V_{rev}=10$ V and $\beta=0.15$ K/s (solid line). The TSCAP spectrum (dashed line and arbitrary units) measured with the same heating rate is shown in the plot in order to compare the relative positions of spectral features.

Table 1
Summary of the observed energy levels together with the results from data analysis

Level	Defect	E (eV)	σ ($\cdot10^{-15}$ cm^{-2})	N_t ($\cdot10^{15}$ cm^{-3})	Notes
E_1	Shallower N	~0.05[a]	–	1.1	Observed only by current techniques.
E_2	Deeper N	0.1±0.01	10–200		(E,σ) deduced from Arrhenius plot. Overall N_t from $C(V)$ at 300 K.
E_3	–	0.15±0.01	~0.01	<0.1	
E_4	$Z_{1/2}$	0.63–0.67[a]	3–20[a]	<0.01	
H_1	–	0.11±0.01	0.01–0.1	0.2	Data from I-DLTS, TSC and TSCAP correlation. Not observed by C-DLTS.
H_2	Shallower B	0.28±0.01	0.2–1	0.04–0.1	(E,σ) from Arrhenius plot.
H_3	Deeper B	0.58–0.63[a]	10–100[a]	<0.01	

The superscript a indicates data taken from literature—these cases were checked for agreement with our measurements.

measurement without performing any further injection. Thus, this measurement is influenced by the charge trapped by H_2 alone, which starts as filled and emits at 120 K, and not by the charge trapped by H_1, which discharged during the first heating. This measurement allows one to isolate the contribution of H_2. The trap concentrations can be estimated from TSCAP spectra using the formula:

$$N_t = N_d \frac{(C_i^2 - C_f^2)}{C_i^2}, \quad (1)$$

where N_t is the trap concentration, and C_i and C_f are the capacitance values measured before and after trap discharge. If the background capacitance $C(T)$ varies during deep level emission, this fact must be accounted for when evaluating C_i and C_f. In our situation, C_i is the maximum value of capacitance before hole emission, while C_f is the capacitance measured at the same temperature when the trap is not filled. The difference, $C_i - C_f$, is indicated by vertical bars in the inset. We find $N_t \approx 2 \cdot 10^{14}$ cm^{-3} for H_1 and $N_t \approx 5 \cdot 10^{13}$ cm^{-3} for H_2. The latter estimate agrees well with C-DLTS results.

The shallower nitrogen level cannot be observed by measuring the junction capacitance as pointed out earlier. To gain further information, we carried out current measurements (i.e. TSC and I-DLTS). Fig. 5 shows the I-DLTS signal measured in the temperature range 20–300 K. We used $t_1 = 1$ ms and $t_2 = 9$ ms for the sampling times, and $t_p = 10$ ms for the injection time. Note that the position of the peaks in I-DLTS and C-DLTS spectra do not match. They differ because the sampling times are different and the signals are described by slightly different equations. N ionization distorts the feature below 50 K. In this case, the N signal exhibits a double peak structure due to the emissions from shallow (E_1) and deep (E_2) nitrogen levels. The peak labeled as H_2 at 180 K relates to shallow boron. Two other peaks are observed near 80 K and 160 K, which are assigned to levels H_1 and E_3, respectively. The position and the shape of the E_3 peak are consistent with the signature previously estimated.

The result of the TSC measurements in the range 20–80 K is shown in Fig. 6. At temperatures higher than 80 K, the background current swamps the weak signal coming from deep levels. Since the heating rate used in these experiments is the same adopted in TSCAP, the peak of the TSC spectrum and the inflection point in the TSCAP spectrum occur at the same temperature. The feature around 30–40 K is due to nitrogen. In this case, the N signal also exhibits a double peak structure. The peak due to H_1 seen near 60 K satisfies both TSC and I-DLTS measurements [35]: $E = 0.11$ eV, $\sigma = 0.1–1 \cdot 10^{-16}$ cm^2. Since the activation energy of aluminum in 4H SiC is 0.19 eV [20,21], neither H_1 nor H_2 relate to Al, which is the p-type doping impurity in our sample. All these results are summarized in Table 1.

4. Conclusions

TSC, TSCAP DLTS current and capacitance measurements were carried out on 4H SiC p^+/n diodes obtained by Aluminum ion implantation on a nitrogen doped n-type epitaxial substrate. The measurements were done over a wide temperature range, 20–400 K, to investigate the material quality of these devices.

Several charge emissions below room temperature related to dopants and impurities were observed. The deeper nitrogen level was observed in all spectra near 0.1 eV. Moreover, the shape of the TSC and I-DLTS signals exhibits a double peak structure because the shallower nitrogen level close to 50 meV was superimposed on the deeper level in current spectra. To our knowledge, this is the first time the TSC/DLTS peaks related to these two energy levels were observed. We estimated the capture cross section of deep nitrogen to be $(1–20) \cdot 10^{-14}$ cm^2.

A clear signal was observed in all the spectra at higher temperatures corresponding to the level labeled here as H_2. From C-DLTS and TSCAP, we inferred this was a hole trap with a concentration $N_t = 0.4–1 \cdot 10^{14}$ cm^{-3}. The signature of this level is $E = 0.28$ V, $\sigma \sim 1 \times 10^{-15}$ cm^2. This signal is related to the shallower level of boron. The hole trap H_3 detected by C-DLTS close to room temperature is related to deep boron, thus confirming a boron contamination occurred during crystal growth.

A hole trap (H_1) with concentration $N_t = 2 \times 10^{14}$ cm^{-3} was also observed. The signature was found to be $E = 0.11 \pm 0.1$ eV, $\sigma = 0.1–1 \times 10^{-16}$ cm^2. To our knowledge, there is no evidence of such a hole trap in literature.

The emission from the $Z_{1/2}$ level, the dominant level produced by irradiation of ion implant, is extremely weak denoting a concentration of $\sim 10^{12}$ cm^{-3}. This confirms the quality of the implant process and of the additional annealing procedures making these devices particularly attractive for future use in particle detection and optoelectronic applications.

Acknowledgments

The authors wish to thank the clean room staff of both "CNR-IMM Sezione di Bologna" and INSA-CEGELy of Lyon for the preparation of the devices. Moreover, the authors are grateful to Antonio De Sio, Andrea Baldi (University of Florence, Italy) and Jessica Metcalfe (SCIPP-University of California Santa Cruz, CA, USA) for technical assistance, and to Ioana Pintilie (University of Bucharest, Romania), Antonella Poggi and Andrea Scorzoni (CNR-IMM Bologna, Italy) for helpful discussions and suggestions. This work was performed partially in the framework of the CERN RD50 Collaboration.

References

[1] A. Elasser, M.H. Kheraluwala, M. Ghezzo, R.L. Steigerwald, N.A. Evers, J. Kretchmer, T.P. Chow, IEEE Trans. Ind. Appl. 39 (2003) 915.
[2] P. Tobias, B. Golding, R.N. Ghosh, IEEE Sens. J. 2 (2003) 543.
[3] J. Eriksson, N. Rorsman, H. Zirath, IEEE Trans. Microwave Theor. Tech. 51 (2003) 796.
[4] M. Bruzzi, et al., Nucl. Instum. Methods A 541 (2005) 189.
[5] F. Nava, P. Vanni, M. Bruzzi, S. Lagomarsino, S. Sciortino, G. Wagner, C. Lanzieri, IEEE Trans. Nucl. Sci. 51 (2004) 238.
[6] T. Kimoto, N. Miyamoto, A. Schone, A. Saitoh, H. Matsunami, K. Asano, Y. Sugawara, J. Appl. Phys. 91 (2002) 4242.
[7] N. Ramungul, V. Khemka, R. Tyagi, T.P. Chow, M. Ghezzo, P.G. Neudeck, J. Kretchmer, W. Hennessy, D.M. Brown, Solid State Electrochem. 42 (1998) 17.

[8] O. Takemura, T. Kimoto, H. Matsunami, T. Nakata, M. Watanabe, M. Inoue, Mat. Sci. Forum (1998) 701.
[9] U. Zimmermann, A. Hallen, B. Breitholtz, Mat. Sci. Forum (2000) 1323.
[10] D.V. Lang, J. Appl. Phys 45 (1974) 3023.
[11] P. Blood, J.W. Orton, The Electrical Characterization of Semiconductors: Majority Carriers and Electron States, Academic Press, London, 1992.
[12] B.W. Wessels, J. Appl. Phys. 47 (1976) 1131.
[13] H. Hurtes, M. Boulou, A. Mitonneau, D. Bois, Appl. Phys. Lett. 32 (1978) 821.
[14] M.G. Buheler, Solid State Electrochem. 15 (1972) 69.
[15] R. Nipoti, F. Moscatelli, A. Scorzoni, A. Poggi, G.C. Cardinali, M. Lazar, C. Raynaud, D. Planson, M.L. Locatelli, J.P. Chante, Mater. Res. Soc. Symp. Proc. 742 (2003) 303.
[16] C. Raynaud, M. Lazar, D. Planson, J. Chante, Z. Sassi, Mater. Scien. Forum 457–460 (2004) 1033.
[17] D. Menichelli, et al., Phys. Rev., B 70 (2004) 195209.
[18] M.E. Dunn in "Electrical characterization of 4-H siC p–n junction diodes" in "Materials Sciences: Crystallography" (http://www.stormingmedia.us/75/7589/A758903.html).
[19] M. Ikeda, H. Matsunami, T. Tanaka, Phys. Rev., B 22 (1980) 2842.
[20] Götz, A. Schöner, G. Pensl, I.W. Suttrop, W.J. Choyke, R. Stein, S. Leibenzeder, J. Appl. Phys. 73 (1993) 3332.
[21] T. Kimoto, A. Itoh, H. Matsunami, S. Sridhara, L.L. Clemen, R.P. Devaty, W.J. Choyke, T. Dalibor, C. Peppermüller, G. Pensl, Appl. Phys. Lett. 67 (1995) 2833.
[22] Z.Q. Fang, D.C. Look, A. Saxler, W.C. Mitchel, Physica B 308–310 (2001) 706.
[23] J.L. Zhang, J.P. Storasta, N.T. Son, E.J. Janzen, J. Appl. Phys. 93 (2003) 4708.
[24] L. Patrick, W.J. Choyke, Phys. Rev., B 5 (1972) 3253.
[25] S.G. Sridhara, L.L. Clemen, R.P. Devaty, W.J. Choyke, D.J. Larkin, H.S. Kong, T. Troffer, G. Pensl, J. Appl. Phys. 83 (1998) 7909.
[26] B. Aradi, P. Dea´k, N.T. Son, E. Janze´n, W.J. Choyke, R.P. Devaty, Appl. Phys. Lett. 79 (2001) 2746.
[27] T. Dalibor, G. Pensl, T. Kimoto, H. Matsunami, S. Sridhara, R.P. Devaty, W.J. Choyke, Diamond Relat. Mater. 6 (1997) 1333.
[28] L. Storasta, F.H.C. Carlsson, S.G. Sridhara, J.P. Bergman, A. Henry, T. Egilsson, A. Hallen, E. Janzen, Appl. Phys. Lett. 78 (2001) 46.
[29] A. Kawasuso, F. Redmann, R. Krause-Rehberg, M. Weidner, T. Frank, G. Pensl, P. Sperr, W. Triftshauser, H. Itoh, Appl. Phys. Lett. 79 (2001) 3950.
[30] M. Weidner, T. Frank, G. Pensl, A. Kawasuso, H. Itoh, R. Krause-Rehberg, Physica B 308–310 (2001) 633.
[31] T. Kimoto, A. Itoh, H. Matsunami, Appl. Phys. Lett. 67 (1995) 2385.
[32] C.G. Hemmingsson, N.T. Son, A. Ellison, J. Zhang, E. Janze´n, Phys. Rev., B 58 (1998) R10119.
[33] G. Pensl, T. Frank, M. Krieger, M. Laube, S. Reshanov, F. Schmid, M. Weidner, Physica B 340–342 (2003) 121.
[34] C. Hemmingsson, N.T. Son, O. Kordina, J.P. Bergman, E. Janzén, J.L. Lindström, S. Savage, N. Nordell, J. Appl. Phys. 81 (1997) 6155.
[35] D. Menichelli, E. Borchi, J. Appl. Phys. 93 (2003) 390.